


**High-magnetic-confinement mode in partially magnetized  $E \times B$  plasmas**

June Young Kim<sup>✉\*</sup>, Jaeyoung Choi<sup>✉</sup>, Y. S. Hwang, and Kyoung-Jae Chung<sup>✉†</sup>  
*Department of Nuclear Engineering, Seoul National University, Seoul, Korea*

 (Received 18 January 2022; accepted 17 April 2022; published 12 May 2022)

The suppression of the gradient-drift driven instability and the transition to the high-magnetic-confinement mode are experimentally observed in a cylindrical partially magnetized  $E \times B$  plasma using an additional biasable electrode installed at the radial edge. When a positive voltage is applied to the electrode, an electron-loss channel forms in its direction, breaking the spatially symmetric nonambipolar flow. Finally, in the steady state, the plasma density tends to peak in the plasma core, approaching plasma densities that are four times larger than those observed in the case where the instability is the strongest. A high-magnetic-confinement mode with a reduced edge-to-center density ratio of 0.16 is observed, which demonstrates that the saturation of magnetic confinement due to the gradient-drift driven instability can be prevented by an asymmetric nonambipolar flow.

DOI: [10.1103/PhysRevE.105.L053202](https://doi.org/10.1103/PhysRevE.105.L053202)

*Introduction.* Magnetized plasma is rife with instability. Most plasmas in the universe and in objects of interest on Earth are strongly magnetized such that the typical magnitudes of gyro radii of both electrons and ions are small compared to the size of the system [1]. Magnetized plasma is a complex system with varying degrees of freedom in which different forms of energy interact. Different coupling mechanisms involved in the dynamics of plasma perturbations facilitate these interactions. Consequently, even minor perturbations can cause instability or the formation of plasma waves. Such plasmas are subject to a wide spectrum of instabilities with wavelengths comparable to the particle gyro scale, which complicate the confinement of a system [2].

In recent years, research on plasma instability has progressed mainly owing to its importance in plasma confinement in fusion research or large linear devices [3,4]. Moreover, there has been widespread interest in such phenomena occurring within small  $E \times B$  devices in other fields of application including electric propulsion and industrial production, which employ diverse plasma processes [5–15]. Recently, there has been an increase in academic and industrial interest toward magnetic confinement and instability in partially magnetized plasma, that is, plasma in which electrons are magnetized, whereas ions are not. To confine electrons and maximize the discharge efficiency in such partially magnetized plasmas, an electric field perpendicular to the external magnetic field is applied. When the plasma density and electric potential are nonuniform across the magnetic field, electron drift combined with the inertial response of unmagnetized ions results in an eigenmode of partially magnetized plasma, which is known as the anti-drift mode [9]. This mode is the basis for the various instabilities that exist in a partially magnetized plasma, which are collectively referred to as gradient-drift driven instabilities.

Gradient-drift driven instabilities originating from ambipolar electric fields aligned with density gradients perpendicular to the magnetic-field line have recently received renewed attention in linear instability studies [9], and comprehensive considerations have been proposed as a part of the theory of the gradient-drift instability [8,10–12]. Notably, partially magnetized plasmas have a chamber dimension comparable to the Lamor radius of their ions, implying that boundary effects are important in the formation of instabilities. A recent theoretical study emphasized that the presence of a finite resistivity in the system modifies the growth rate and angular frequency of the instability owing to current conservation at the bounding walls [11,12].

In addition to these theoretical efforts, the importance of boundaries on the overall characteristics of the Simon-Hoh instability has been emphasized through experiments [13]. Aligning the electric boundary perpendicular to the magnetic-field line was shown to strongly influence the spoke instability in the  $E \times B$  Penning discharge. Enhanced diffusion along the conductive boundary (i.e., Simon's short-circuit effect) reduces the radial electric field, indicating that spoke oscillations are suppressed at the metal wall boundary. Hence, the turbulent flux can be reduced to the classical flux ratio across the magnetic field by lowering the magnitude of the instability. However, this instability reduction method decreases the plasma density because of the significant loss in magnetic-field-aligned electrons as a result of the short-circuit effect. The causal relationship between the mitigation of the gradient-drift driven instability and enhancement of magnetic confinement in partially magnetized plasmas remains unknown.

The aforementioned issues form the motivation behind this Letter. Identifying the direct relationship between magnetic confinement and instability in partially magnetized plasmas is critical for understanding instability characteristics and will be a breakthrough in plasma physics in consonance with the development of various application fields. We present the results of instability-suppression experiments focusing on a

\*ptcbcg@gmail.com

†jkjsh1@snu.ac.kr

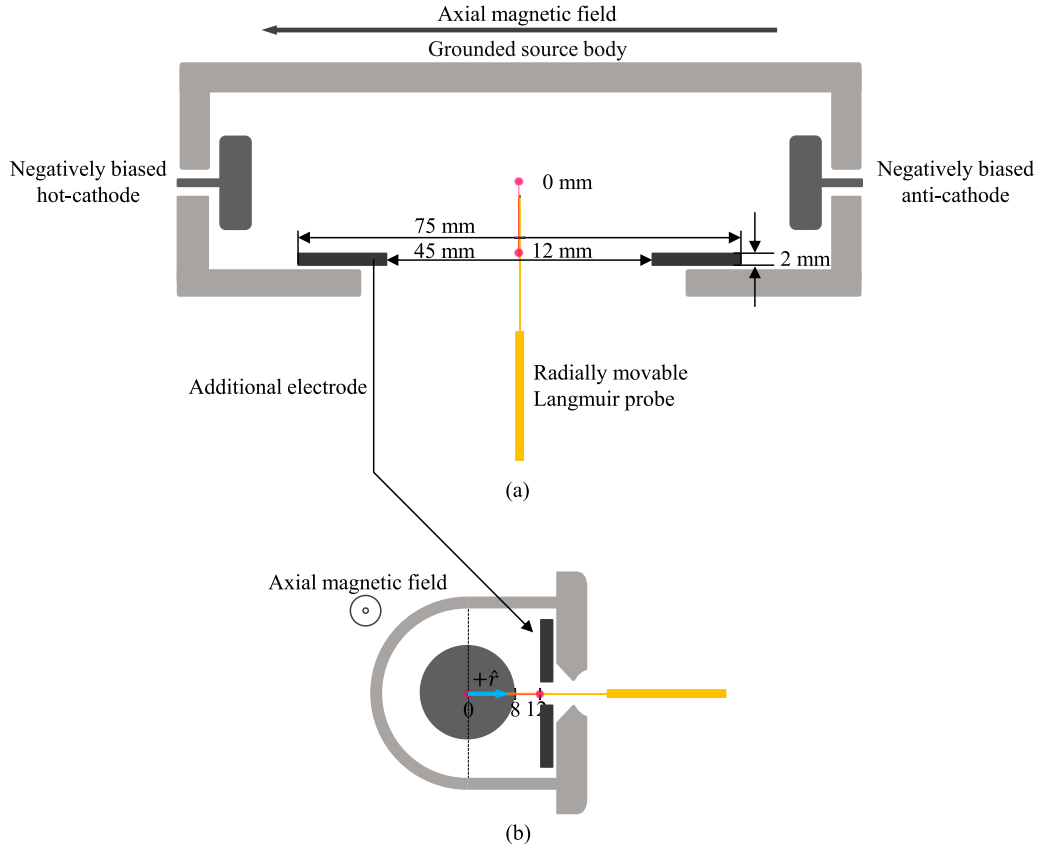


FIG. 1. Cross section of a partially magnetized  $E \times B$  Penning discharge source seen from (a) above and (b) the side with a radially movable single Langmuir probe [14]. The blue arrow in (b) indicates the radial direction, and the red line indicates the measurement range.

nonambipolar flow, which improve our understanding of the causal relationship between “two physical phenomena” in a device that demonstrates the Simon-Hoh instability and saturation of magnetic confinement [14].

**Results and Discussion.** As shown in Fig. 1, the partially magnetized plasma source used in this Letter has two main regions: the hot-cathode region and the extraction region [14,15]. The hot-cathode region (8 mm from the radial center) is a near-cylindrical area with two axial boundaries (hot-cathode and anti-cathode). The extraction region is the region outside the hot-cathode region (8–14 mm). The beam-plasma discharge is a well-known mechanism for initiating discharges in the hot-cathode regions as described in our previous study on  $E \times B$  Penning discharges [14,15]. The inner wall of the source is connected to the ground and serves as the reference potential for the entire plasma source system. An additional electrode made of tungsten was installed on one side of the radial edge in the extraction region to control the nonambipolar flow. The radial position ranged from 12 to 14 mm in the extraction region and almost covered the grounded plate.

The spatial changes in the plasma parameters were calculated using the electron energy probability functions (eepfs). The experiments were performed at a magnetic-field strength  $B_z$  of 147 G and an argon pressure of 0.46 mTorr. The cathode voltage was fixed at  $-60$  V, and the current was 3.0 A with a 10% variation. The disappearance of the beam component and isotropization of the eepfs were ensured for all experimental conditions, satisfying the conditions for the

application of the Druyvesteyn method [14–17]. The plasma is collisionless at the relevant length scale (i.e., the probe tip radius of 0.15 mm and the Debye length of 0.02 mm must be less than the electron-neutral collisional mean free path; 1 m at 0.46 mTorr). The second derivative of the current-voltage curve  $I''_e(\varepsilon)$  is proportional to  $e\text{epf } f_e(\varepsilon)$  as follows:  $f_e(\varepsilon) = 2m_e/(e^2A)(2/m_e)^{1/2}I''_e(\varepsilon)$ , where  $m_e$ ,  $e$ ,  $\varepsilon$ , and  $A$  are the electron mass, elementary charge, electron energy in volts, and probe area, respectively [17]. The electron density  $n_e$  and effective electron temperature  $T_{\text{eff}}$ , corresponding to the mean electron energy are determined by integrating the eepf as follows:  $n_e(\varepsilon) = \int_0^\infty \varepsilon^{1/2} f_e(\varepsilon) d\varepsilon$  and  $T_{\text{eff}} = 2/3 \int_0^\infty \varepsilon^{3/2} f_e(\varepsilon) d\varepsilon / \int_0^\infty \varepsilon^{1/2} f_e(\varepsilon) d\varepsilon$ . The plasma potential  $V_p$  is determined by the zero-crossing point of  $I''_e(\varepsilon)$ . A time-integration method with a timescale longer than the instability scale was applied to minimize the effect of plasma fluctuation, and the error bar of the measured  $V_p$  was below 0.5%.

The instability was measured using an electrically floated Langmuir probe located 10 mm from the radial center, and the frequency spectra were obtained by performing fast Fourier transforms (FFTs) on the signal recorded by the Langmuir probe. The Langmuir probe was terminated by a 1 M $\Omega$  resistor to an oscilloscope, and the Hanning window function was used to avoid spectral leakage. The frequency  $f$  corresponding to the maximum magnitude of the FFTs was defined as the dominant frequency. Figures 2(a) and 2(b) show the FFT results and current signal used to identify instability suppression. The absolute values of the floating potential of the two

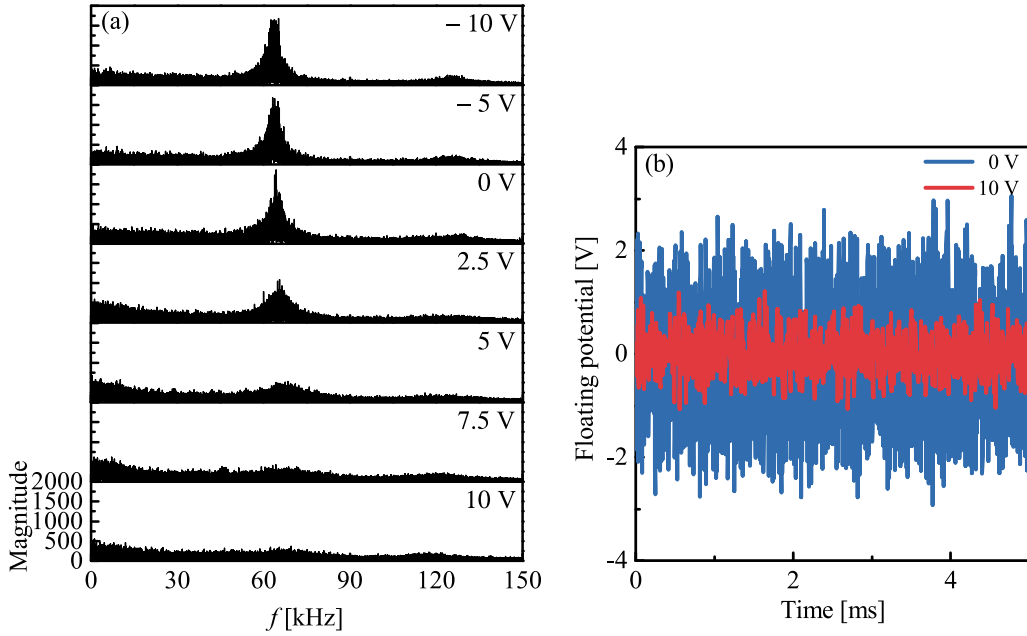


FIG. 2. (a) Frequency spectra for the range of voltages applied to the additional electrode  $V_E$  of interest and (b) time series of the floating potential at  $V_E = 0$  and 10 V.

experimental results were shifted to simplify the comparison of the fluctuation level. Figure 3(a) shows that the dominant frequency of fluctuation is approximately constant at 64 kHz along the radial direction, which has been previously demonstrated to be the collisionless Simon-Hoh instability [14]. When a positive bias voltage was applied to the additional electrode, the fluctuation became undetectable; plasma instability was significantly reduced inside the ion source as depicted in Fig. 3(b).

The radial profile of plasma parameters, namely,  $n_e$ ,  $T_{\text{eff}}$ , and  $V_p$ , exhibits nonuniform characteristics as shown in Figs. 4(a)–4(c). An increase in  $V_E$  significantly affects  $n_e$  and

$V_p$ ;  $n_e$  substantially increases along with the plasma potential locked to  $V_E$  near the additional electrode.

The self-generated ambipolar potential causes an  $\mathbf{E} \times \mathbf{B}$  drift, which can destabilize the anti-drift mode if  $\frac{\omega_{\text{dia}}}{\omega_{\mathbf{E} \times \mathbf{B}}} > 0$  for  $\omega < \omega_{\mathbf{E} \times \mathbf{B}}$ , where  $\omega_{\text{dia}}$  is the diamagnetic drift frequency and  $\omega_{\mathbf{E} \times \mathbf{B}}$  is the  $\mathbf{E} \times \mathbf{B}$  drift frequency [9]. Then, the excitation condition of the collisionless Simon-Hoh instability is  $\nabla n_e \cdot \mathbf{E}_r > 0$ , where  $\mathbf{E}_r$  is the radial electric field calculated by the  $V_p$  structure. Notably, as  $V_E$  increases,  $\nabla n_e \cdot \mathbf{E}_r > 0$  ( $\frac{\omega_{\text{dia}}}{\omega_{\mathbf{E} \times \mathbf{B}}} > 0$ ) remains satisfied near the periphery of the hot cathode where the magnitude of the FFT is maximum at  $V_E = 0$  V as shown in Fig. 5(a).

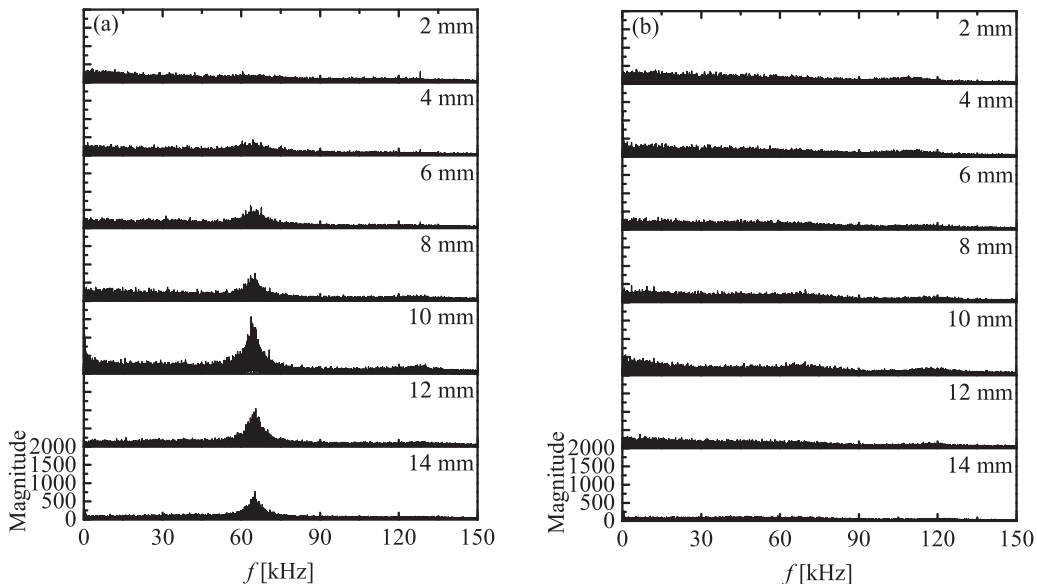


FIG. 3. Radial profile of FFT results at (a)  $V_E = 0$  V and (b)  $V_E = 10$  V.

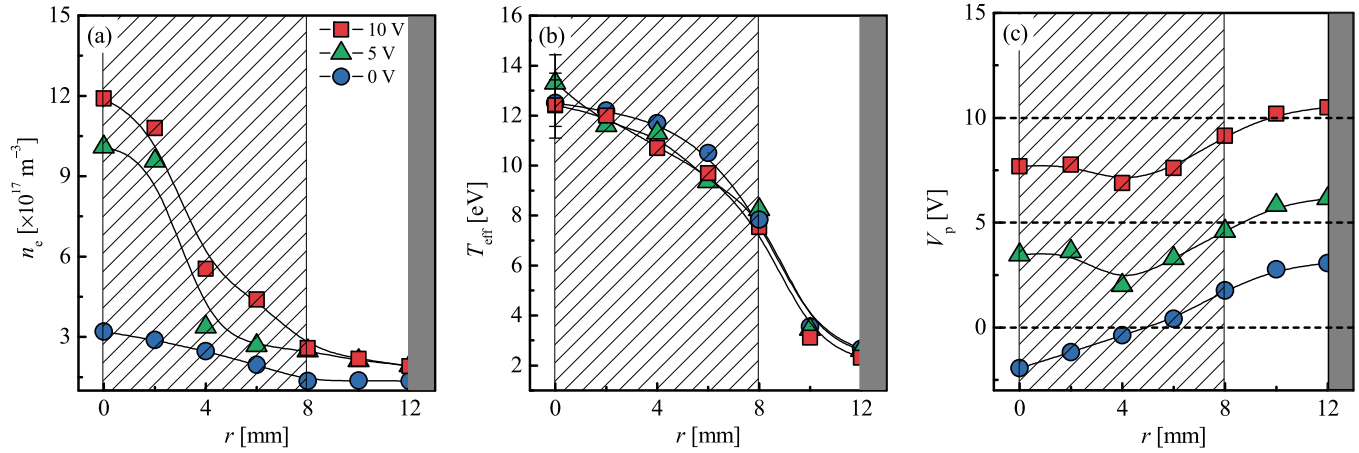


FIG. 4. Radial profile of plasma parameters measured by a single Langmuir probe on the additional electrode at voltages  $V_E$  of 0, 5, and 10 V. (a) Electron density  $n_e$ , (b) effective electron temperature  $T_{\text{eff}}$ , and (c) plasma potential  $V_p$ . The hot-cathode region where energetic electrons are generated is indicated by the shaded area, and the location of the additional electrode is indicated at 12 mm.

The rate at which the discharge power increases should be examined to monitor global energy balance. When  $V_E = 5$  V, the power increase rate is approximately 5% compared to when  $V_E = 0$  V, whereas the density increase rate reaches 206% at the radial center. Accordingly, the suppression of the instability and detection of the high-magnetic-confinement mode are described by changes in the spatial flow of charged particles. The breaking of a spatially symmetric nonambipolar flow can be explained by a variation in the particle loss channel. When the additional electrode was grounded, both the chamber wall and the additional electrode functioned as anodes, and all azimuthal directions were designated as electron and ion loss channels. Meanwhile, electrons cannot be lost to the axial cathode, indicating that the unique property of this partially magnetized plasma source is dominated by the spatially symmetric global nonambipolar flow. At  $V_E = 0$  V, the ratio of the cathode current (3 A) to the current flowing through the grounded additional electrode (0.78 A) is approximately 26%. Considering the area ratio between the additional electrode and the inner wall of the grounded

chamber (approximately three times the difference in area), it is estimated that a uniform current of approximately 3 A is distributed between the grounded chamber wall and the additional electrode (i.e., the current densities of the chamber inner wall and the additional electrode are nearly identical). That is, the absolute values of the cathode and anode currents are the same, which is an intrinsic characteristic of the Penning source.

When the additional electrode is positively biased, the local electron loss to the additional electrode increases rapidly, and the plasma potential is also locked to a positive voltage. At the location of the additional electrode (12 mm), the difference between the anode and the plasma potentials is less than the electron temperature ( $\Delta V_p$  is 1.15 and 0.5 V when  $V_E$  is 5 and 10 V, respectively). Therefore, electrons near the additional electrode can overcome the potential difference and be lost to the electrode. The current flow to the additional electrode increased steadily as  $V_E$  increased, and when  $V_E$  reached 10 V, most of the electron current flowed to the additional electrode (95% of the discharge current). These

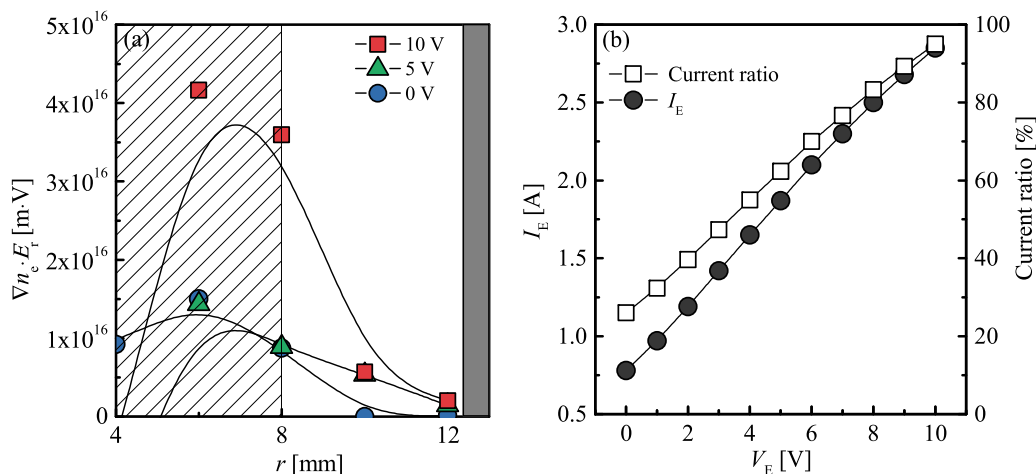


FIG. 5. (a) Radial variation of the excitation condition of the collisionless Simon-Hoh instability  $\nabla n_e \cdot E_r$  at different applied voltages  $V_E$ , and (b) recorded current through the additional electrode  $I_E$ , and the ratio of  $I_E$  to the discharge current (3 A).

experimental observations indicate that during the transition to the high-confinement mode, particle fluxes have multiple spatially asymmetric paths for a typical plasma density and temperature in the wall boundary as demonstrated by a study of tokamaks [18]. That is, the occurrence of the gradient-drift-induced instability in a cylindrical geometry not only requires axial symmetry of the chamber geometry, plasma density, temperature, and electric field but also requires axial symmetry of the flux near the boundary, which has been overlooked in past experimental studies on partially magnetized plasmas.

The edge-to-center density ratio ( $h$  factor) is a measure of the ratio of the plasma density at the plasma-sheath edge to that at the discharge center and is used to estimate the plasma loss to the boundary. Recently, Kim *et al.* used the  $h$  factor for the partially magnetized  $E \times B$  Penning source used in this Letter to observe magnetic confinement changes [14]. Accordingly, the  $h$  factor measured in previous studies was compared with that of this Letter. In a previous study at 0.9 mTorr where the collisionless Simon-Hoh instability was significant, the  $h$ -factor ( $h_r$ ) reached asymptotic values, indicating a saturation of magnetic confinement as shown in Fig. 6. That is, cross-field transport at a low pressure becomes active owing to the instability combined with rotation. In this Letter when the instability was suppressed ( $V_E = 10$  V), the  $h$  factor was considerably reduced, indicating the appearance of a high-confinement mode. Finally, it can be concluded that the suppression of instability via asymmetric nonambipolar flows increases magnetic confinement.

**Conclusion.** In conclusion, we discovered that a spatially asymmetric nonambipolar flow can suppress the gradient-drift driven instability and the transition to a high-magnetic-confinement mode. The positively biased additional electrode effectively breaks the spatial symmetry of the global flow of electrons and ions. Finally, the asymmetric flow suppresses the excitation of the gradient-drift driven instability, enhancing magnetic confinement. We believe that the boundary plays a significant role in the formation and control of instabilities in partially magnetized plasmas, and we demonstrate the relevance of the boundary-induced effect in improving yields in plasma applications. Since the structure and electrical

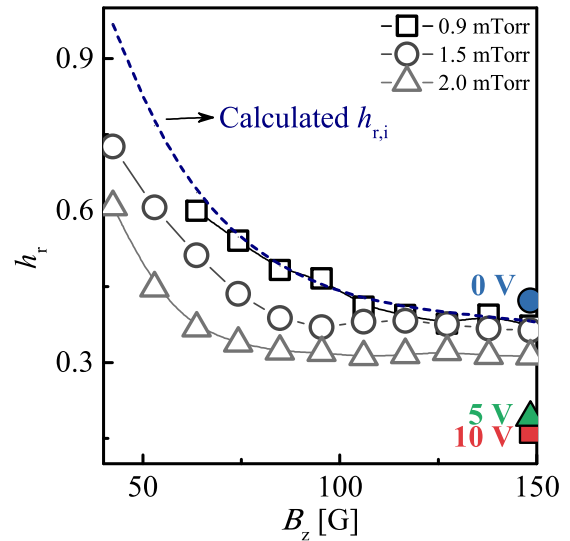


FIG. 6. Data from a previous study [14] and a comparison with the present Letter. Edge-to-center density ratio  $h_r$  plotted against different magnetic field strengths  $B_z$  and pressures. The dashed line is the estimated  $h$  factor at a high magnetic field considering instability-enhanced cross-field transport [14]. We newly plotted the ratio of the plasma density at a distance of 12 mm to that at the center for different applied voltages  $V_E$  at 147 G.

connection of the  $E \times B$  devices are designed to target the symmetry of plasma parameters, this Letter proposes that symmetry breaking of the plasma in terms of the flow can provide a breakthrough in terms of achieving high device stability and efficiency.

**Acknowledgments.** We thank I. Kaganovich (Princeton Plasma Physics Laboratory) for an informative discussion. This research was supported by the Basic Science Research Program through the National Research Foundation of Korea (NRF) funded by the Ministry of Science, ICT, and Future Planning (Grant No. 2020R1C1C1009547) and partly by the NRF funded by the Korean government (MSIT) (Grant No. 2019M2D1A1080261).

The authors declare no competing interests.

- [1] B. D. Melrose, *Instabilities in Space and Laboratory Plasmas* (Cambridge University Press, Cambridge, UK, 1986).
- [2] A. Hasegawa, *Physics and Chemistry in Space, Plasma Instabilities and Nonlinear Effects* (Springer, Berlin/Heidelberg, 2012), Vol. 8.
- [3] K. H. Burrell, Effects of  $E \times B$  velocity shear and magnetic shear on turbulence and transport in magnetic confinement devices, *Phys. Plasmas* **4**, 1499 (1997).
- [4] M. Porkolab, V. Arunasalam, and R. A. Ellis, Jr., Parametric Instability and Anomalous Heating Due to Electromagnetic Waves in Plasma, *Phys. Rev. Lett.* **29**, 1438 (1972).
- [5] D. Kaganovich, A. Smolyakov, Y. Raitses, E. Ahedo, I. G. Mikellides, B. Jorns, F. Taccogna, R. Gueroult, S. Tsikata, A. Bourdon, J. P. Boeuf, M. Keidar, A. T. Powis, M. Merino, M. Cappelli, K. Hara, J. A. Carlsson, N. J. Fisch, P. Chabert,

- I. Schweigert, T. Lafleur, K. Matyash, A. V. Khrabrov, R. W. Boswell, and A. Fruchtman, Physics of  $E \times B$  discharges relevant to plasma propulsion and similar technologies, *Phys. Plasmas* **27**, 120601 (2020).
- [6] J.-P. Boeuf and M. Takahashi, Rotating Spokes, Ionization Instability, and Electron Vortices in Partially Magnetized  $E \times B$  Plasmas, *Phys. Rev. Lett.* **124**, 185005 (2020).
- [7] T. Powis, J. A. Carlsson, I. D. Kaganovich, Y. Raitses, and A. Smolyakov, Scaling of spoke rotation frequency within a Penning discharge, *Phys. Plasmas* **25**, 072110 (2018).
- [8] O. Koshkarov, A. Smolyakov, Y. Raitses, and I. Kaganovich, Self-Organization, Structures, and Anomalous Transport in Turbulent Partially Magnetized Plasmas with Crossed Electric and Magnetic Fields, *Phys. Rev. Lett.* **123**, 239903 (2019).

- [9] I. Smolyakov, O. Chapurin, W. Frias, O. Koshkarov, I. Romadanov, T. Tang, M. Umansky, Y. Raitses, I. D. Kaganovich, and V. P. Lakhin, Fluid theory and simulations of instabilities, turbulent transport and coherent structures in partially-magnetized plasmas of  $E \times B$  discharges, *Plasma Phys. Controlled Fusion* **59**, 014041 (2016).
- [10] W. Villafana, F. Petronio, A. C. Denig, M. J. Jimenez, D. Eremin, L. Garrigues, F. Taccogna, A. Alvarez-Laguna, J.-P. Boeuf, A. Bourdon, P. Chabert, T. Charoy, B. Cuenot, K. Hara, F. Pechereau, A. Smolyakov, D. Sydorenko, A. Tavant, and O. Vermorel, 2D radial-azimuthal particle-in-cell benchmark for  $E \times B$  discharges, *Plasma Sources Sci. Technol.* **30**, 075002 (2021).
- [11] V. Morin, Sheath boundary effects on the stability of Hall plasmas, Doctoral dissertation, University of Saskatchewan, 2018.
- [12] V. Morin and A. I. Smolyakov, Modification of the Simon-Hoh instability by the sheath effects in partially magnetized  $E \times B$  plasmas, *Phys. Plasmas* **25**, 084505 (2018).
- [13] E. Rodríguez, V. Skoutnev, Y. Raitses, A. Powis, I. Kaganovich, and A. Smolyakov, Boundary-induced effect on the spoke-like activity in  $E \times B$  plasma, *Phys. Plasmas* **26**, 053503 (2019).
- [14] J. Y. Kim, J. Y. Jang, J. Choi, J. I. Wang, W. I. Jeong, M. A. I. Elgarhy, G. Go, K. J. Chung, and Y. S. Hwang, Magnetic confinement and instability in partially magnetized plasma, *Plasma Sources Sci. Technol.* **30**, 025011 (2021).
- [15] J. Y. Kim, W. I. Jeong, M. A. I. Elgarhy, J. Choi, G. Go, K. J. Chung, and Y. S. Hwang, Non-Maxwellian electron energy probability functions in an indirectly heated cathode Bernas source, *Appl. Sci. Convergence Technol.* **29**, 167 (2020).
- [16] R. B. Lobbia and B. E. Beal, Recommended practice for use of Langmuir probes in electric propulsion testing, *J. Propul. Power* **33**, 566 (2017).
- [17] M. A. Lieberman and A. J. Lichtenberg, *Lichtenberg Principles of Plasma Discharge and Material Processing*, 2nd ed. (Wiley, Hoboken, NJ, 2005).
- [18] S.-I. Itoh and K. Itoh, Model of L to H-Mode Transition in Tokamak, *Phys. Rev. Lett.* **60**, 2276 (1988).